Journal of Anatomy

J. Anat. (2017) **231**, pp229–247 doi: 10.1111/joa.12632

The effect of age and demographics on rib shape

Sven A. Holcombe,[1,2] Stewart C. Wang[2] and James B. Grotberg[1]

[1]*Department of Biomechanical Engineering, University of Michigan, Ann Arbor, MI, USA*
[2]*International Center for Automotive Medicine, University of Michigan, Ann Arbor, MI, USA*

Abstract

Elderly populations have a higher risk of rib fractures and other associated thoracic injuries than younger adults, and the changes in body morphology that occur with age are a potential cause of this increased risk. Rib centroidal path geometry for 20 627 ribs was extracted from computed tomography (CT) scans of 1042 live adult subjects, then fitted to a six-parameter mathematical model that accurately characterizes rib size and shape, and a three-parameter model of rib orientation within the body. Multivariable regression characterized the independent effect of age, height, weight, and sex on the rib shape and orientation across the adult population, and statistically significant effects were seen from all demographic factors ($P < 0.0001$). This study reports a novel aging effect whereby both the rib end-to-end separation and rib aspect ratio are seen to increase with age, producing elongated and flatter overall rib shapes in elderly populations, with age alone explaining up to 20% of population variability in the aspect ratio of mid-level ribs. Age was not strongly associated with overall rib arc length, indicating that age effects were related to shape change rather than overall bone length. The rib shape effect was found to be more strongly and directly associated with age than previously documented age-related changes in rib angulation. Other demographic results showed height and sex being most strongly associated with rib size, and weight most strongly associated with rib pump-handle angle. Results from the study provide a statistical model for building rib shapes typical of any given demographic by age, height, weight, and sex, and can be used to help build population-specific computational models of the thoracic rib cage. Furthermore, results also quantify normal population ranges for rib shape parameters which can be used to improve the assessment and treatment of rib skeletal deformity and disease.

Key words: Rib shape; Geometry; Age; Spiral.

Introduction

Rib fractures and chest injuries are particularly problematic for elderly individuals. They experience both a greater likelihood of sustaining fractures compared with younger cohorts (Kent et al. 2008) and poorer clinical outcomes, including longer stays in intensive care facilities resulting in a greater overall economic burden (Lee et al. 2006). Overall, chest injuries including rib fractures most often occur due to high energy traumatic events, with motor vehicle crashes (MVCs) accounting for between 46 and 65% of severe injuries, falls accounting for 21–27% (Galan et al. 1992; Veysi et al. 2009; Söderlund & Ikonen, 2015). Low energy injuries become more prevalent in the elderly, with falls accounting for 70% of geriatric trauma (Bonne & Schuerer, 2013). Implicating factors in chest injuries have been found, with reduced bone mineral density and heavy alcohol use each contributing to the risk of rib fractures (Wuermser et al. 2011).

In researching such injuries, computational human body models are being increasingly used for impact and injury simulation of the chest and thorax. These models are largely based on the internal anatomy of selected individuals, usually chosen to represent the average external anatomy of a chosen demographic–most often, for example, an average-sized adult male. A recent review of computational models (Hu & Reed, 2012) identifies a current need for a more diverse modeling approach whereby at-risk or vulnerable populations are specifically included in modeling efforts. Elderly occupants, female occupants, obese occupants, and children are all identified as having greater risk of injury in particular body regions. To build such models and provide them the fidelity to model a diverse population, a clear understanding of the geometric variation within the population is required.

Kent et al. (2005) first described an age effect on rib angulation in an adult male population. Ribs were found to

Correspondence
Sven A. Holcombe, Department of Biomechanical Engineering, University of Michigan International Center for Automotive Medicine 3415 Med Sci I, 1150 W. Medical Center Dr. Ann Arbor, MI, 48105, MI, USA. E: svenho@umich.edu

Accepted for publication *5 April 2017*
Article published online *13 June 2017*

rotate more horizontally in the sagittal plane with age, from a ninth rib angle of 50° in an 18-year-old to 57° in an 89-year-old. Further efforts to quantify rib and rib cage shape have followed one of two general methodologies. The first takes landmarks placed strategically across the rib cage from a series of individuals, then uses a combination of generalized Procrustes analysis (GPA) and principal component analysis (PCA) to quantify changes in those landmarks across populations. Gayzik et al. (2008) used GPA to analyze 106 landmarks from 63 adult male rib cages (Slice & Stitzel, 2004; Gayzik et al. 2008) and described a rounding of the rib cage with aging. Weaver et al. (2014) used a similar technique with a more complete set of landmarks across the rib cage, and applied it to a larger population including 164 adults and 175 children to quantify rib cage morphology changes as a whole, reporting increased rib angles and a rounding of the rib cage with age. Shi et al. (2014) and a follow-up study by Wang et al. (2016) applied GPA and PCA to landmarked rib cages from 89 and 101 subjects, respectively, and confirmed an increase in rib angle with age along with increased rib cage depth coupled with reduced rib cage width. Although techniques such as GPA and PCA provide an overall quantification of the rib cage, their results usually combine the changes in bone shape with the changes in bone position and orientation, and the large number of resulting coefficients can be difficult to interpret.

A second general methodology isolates the ribs themselves and characterizes their shapes using measures from geometric primitives. Examples include rib shape representations using a circular ring (Kent et al. 2001), an arc (Schultz et al. 1974), an ellipse (Margulies et al. 1989), and a pair of superimposed arcs (Roberts & Chen, 1972; Roberts, 1977). Two recent models have provided the additional capability of fully recreating the underlying rib shape from their parameters alone. Kindig & Kent (2013) presented a seven-parameter model with a circle and semi-ellipse connected by short patches (Holcombe et al. 2014; Kindig & Kent, 2013). Using connected spirals as the model primitives, Holcombe et al. (2016) provided the additional benefits of simplifying the parameter space (with one less parameter and fewer joining patches), and using parameters that were themselves direct geometric properties of ribs such as their size, aspect ratio, and skewness. This meant that any rib rebuilt using statistically average parameter values from a population would itself reflect the average geometric properties from within that same population. To date, these direct models of rib shape have not been applied to large adult populations for the study of changes with age; however, experimental studies of isolated ribs under loading have reported significant changes in rib stiffness and fracture onset with age (Agnew et al. 2015).

The objective of the current study is to quantify the rib shape and orientation variation present in adults, and to highlight the specific changes in human ribs that come as a result of aging. This was accomplished by applying the six-parameter rib shape model described in Holcombe et al. (2016) along with measures of rib orientation to a large subject pool (20 627 ribs from 507 females and 535 males) that is representative of the adult population. Regression analysis of parameter trends then characterized rib morphology variation by demographic predictors of age, height, weight, and sex, and in particular tested the hypothesis that there is a significant aging effect on the size, shape, and orientation of ribs that occurs independently of other general demographics. A final outcome of this study is a parsimonious model of overall rib shape that allows researchers to build statistically representative rib geometry for any chosen subject demographic.

Material and methods

Study population

Under IRB HUM00041441, human rib centroidal path geometry was extracted from 507 female and 535 male CT scans in the International Center for Automotive Medicine (ICAM) morphomics database. Scans were from adult patients (20–99 years of age) who entered a Level 1 trauma center between 2000 and 2016 and underwent abdomen and/or chest CT scanning as part of their normal course of diagnosis and treatment. Scans exhibiting skeletal abnormality (including scoliosis, kypohosis, spine or rib fixation devices, bifurcating ribs or abnormal rib counts) were excluded, as were fractured ribs (see below). Of the patients meeting scan inclusion criteria, the majority were admitted due to MVCs (78%) and falls (7%). The study population demographics are shown by sex in Fig. 1, and compared with the CDC's anthropometric reference data for North American adults over 20 years of age from 2007–2010 (Fryar et al. 2012) in Table 1, with heights and weights generally differing by <0.1 standard deviations between the current study and the CDC comparison populations.

The in-plane resolution of CT scan images varied between 0.54 and 0.98 mm with a median of 0.70 mm. CT slice spacing varied between 0.625 mm (16% of scans) and 5 mm (18% of scans), with the majority (58%) having slice spacing at 1.25 mm. Demonstration of the relative accuracy of rib centroid position and measurements (described below) taken from these varied scan resolutions is provided as Supporting Information Appendix S1.

Individual ribs present in scan

From the 1042 adult CT scans, a total of 22 004 individual ribs were fully captured within CT scan windows. Ribs with fracture were identified based on radiology reports associated with the CT image or visual inspection and were excluded from analysis, leaving a total of 20 627 included observations. Mid-level ribs were the most commonly fractured and therefore had a greater exclusion rate than other ribs; however, all levels from 2 through 12 retained at least 1600 uninjured ribs as observations.

Rib centroid extraction

Rib centroidal path geometry was extracted for each rib from its corresponding CT scan volume in the form of a series of 3D point coordinates running along its centroidal path (i.e. the sequence of

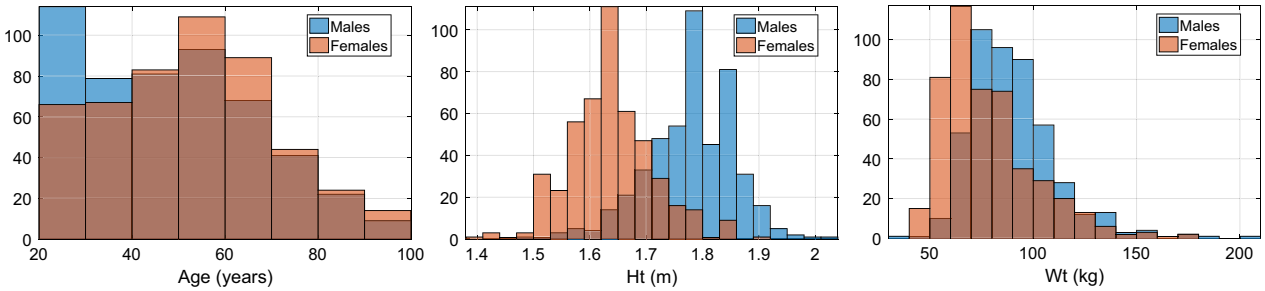

Fig. 1 Population histograms showing the age, height and weight distributions for males and females within the studied population.

Table 1 Study demographics mean and percentiles (in bold), along with CDC reference population data in parentheses (Fryar et al. 2012).

	Mean	SD	5th	10th	25th	50th	75th	90th	95th
Males (n = 535)									
Weight, kg	**89.6**	**21.1**	**63.3**	**68.0**	**75.0**	**86.0**	**100.0**	**115.0**	**132.2**
	(88.7)	(33.8)	(61.5)	(66.5)	(75.0)	(86.1)	(98.9)	(114.4)	(124.1)
Height, cm	**177.9**	**7.7**	**165.0**	**168.0**	**173.0**	**178.0**	**183.0**	**188.0**	**189.2**
	(175.9)	(15.0)	(163.2)	(166.0)	(170.9)	(176.1)	(180.9)	(185.4)	(188.2)
Females (n = 507)									
Weight, kg	**77.9**	**22.4**	**52.0**	**54.8**	**62.0**	**72.0**	**88.0**	**109.2**	**123.0**
	(75.4)	(26.8)	(50.2)	(53.6)	(61.1)	(71.3)	(85.5)	(102.2)	(113.8)
Height, cm	**163.6**	**7.6**	**152.0**	**154.9**	**158.7**	**163.0**	**168.0**	**173.0**	**177.8**
	(162.1)	(10.8)	(150.7)	(153.1)	(157.3)	(162.1)	(166.8)	(170.9)	(173.7)

centroids connecting adjacent cross-sections). The extraction process was performed using semi-automated software written in MATLAB, and is described in detail in Holcombe et al. (2016) and summarized as follows. First, points are manually placed at the rib's head (the end proximal to the spine, specifically on the articulation point between rib and vertebral body) and the rib end distal to the spine (at the apex of the cup-shaped costo-chondral junction). The centroidal path is then extracted by building an initial rib path between end points from an algorithm adapted from Staal et al. (2007), followed by iterative refinement of that path by taking cross-sectional slices through the CT volume and identifying the 2D centroid of filled regions of segmented rib cortical bone.

Rib plane and orientation parameters

A local rib coordinate system was fitted to each set of centroidal path rib points, having its origin at the rib's proximal end landmark, its local x-axis passing through the distal end landmark, and its local y-axis chosen so as to minimize the distance of all rib points from the local x-y plane. Three rotational parameters then define the orientation of this local rib plane with respect to a fixed body coordinate system as shown in Fig. 2.

A rib's pump-handle parameter (α_{PH}) is specified as the angle between the rib local x-axis and the coronal plane. A rib's lateral swing (α_{LS}) is the angle between the rib local x-axis and the sagittal plane, and its bucket-handle angle (α_{BH}; Margulies et al. 1989) is a rotation about the rib's local x-axis after the prior rotations are performed. The convention for α_{BH} was chosen such that rotation moving the lateral aspect of the rib superiorly results in positive α_{BH}, whereas rotation moving the lateral aspect of the rib inferiorly results in negative α_{BH}.

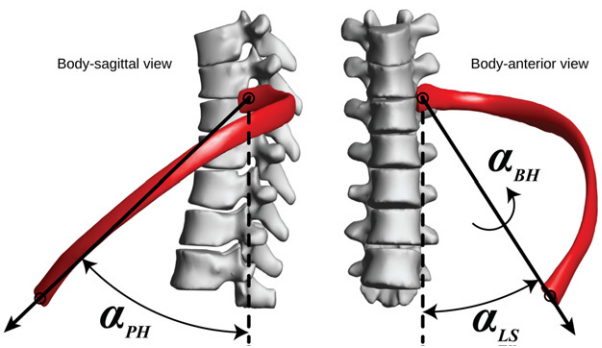

Fig. 2 Rib plane parameterization into pump-handle angle (α_{PH}), lateral swing angle off the mid-sagittal plane (α_{LS}), and bucket-handle angle (α_{BH}).

The combination of these three rotational parameters allows an initial neutrally posed rib (on its correct side yet hanging directly inferiorly) to undergo successive rotations by α_{PH} (up from the sagittal plane), α_{LS} (away from the medial plane), then by α_{BH} (about the newly rotated x-axis, positive for left-sided ribs and negative for right-sided ribs), with the resulting rib being oriented correctly in the body habitus.

To compensate for misalignment between the patient anatomical planes and the global scan coordinate system, a true rib cage lateral vector was created. It is specified as the normal direction to plane of best fit through a point cloud consisting of (i) midpoints of all left and right proximal rib end pairs, (ii) points at the center of each thoracic vertebrae, and (iii) medial points placed along the sternum

and linea alba. Rib plane rotation angles are then defined relative to orthogonal body coronal and sagittal planes derived from this body-lateral vector and the scanning bed.

Rib in-plane parametric shape model

Each rib's overall shape is characterized using a six-parameter rib shape model introduced in Holcombe et al. (2016). Non-linear optimization (performed with MATLAB's Optimization Toolbox) is used to find the set of parameters that minimize the sum-of-squares distance from the original rib points (seen in-plane with respect to its local *x*- and *y*-axes) to the resulting parameter-based rib model path. A full derivation of rib shape from parameters is described in Holcombe et al. (2016), with the parameters illustrated in Fig. 3 and their effects summarized below. Individually, the S_x parameter controls the overall size of a rib by directly prescribing its end-to-end length. The rib's peak is then given by the X-Y pair [X_{Pk}, Y_{Pk}], expressed in coordinates normalized by S_x. Consequently, $1/Y_{Pk}$ describes overall rib aspect ratio in terms of height in the local plane vs. S_x, while X_{Pk} describes 'skewness' of the rib's shape independent of aspect ratio, with a low X_{Pk} moving the rib peak closer to the proximal end, whereas larger X_{Pk} values push this peak towards the distal end. The ϕ_{pia} parameter directly controls the inner angle between the rib's path and the local *x*-axis at the proximal end, and B_d and B_p are logarithmic spiral constants that modulate the local curvature of the rib in its distal and proximal regions, respectively.

Derived shape properties

The shape model parameters include four direct geometric measures (size, aspect ratio, skewness, and proximal inner angle) as part of its parameterization. Five additional geometric properties were measured to further quantify key aspects of the resulting rib shapes. Overall arc length in the local plane (L_{2d}), overall arc length including out-of-plane deviation (L_{3d}), inner angle at the distal end (ϕ_{dia}), and local curvature at both the distal end (κ_{dist}) and posterior extension (κ_{post}) were chosen as additional derived measures, as illustrated in Fig. 4.

The equation for the curvature κ at any given location θ of a logarithmic spiral has the basic form (Weisstein, 2016) given in Eq. (1) below:

$$\kappa = \frac{e^{-B\theta}}{a\sqrt{1+B^2}} \quad (1)$$

where B is the logarithmic constant (B_p for the proximal spiral and B_d for the distal spiral), and a is the scale factor used to transform the unscaled spiral equations from their original [x, y] space to the local rib plane, given in Holcombe et al. (2016).

Substituting those factors along with either B_p or B_d in Eq. (1) we can interrogate any proximal or distal rib location for its local curvature κ (or its radius of curvature, which is $1/\kappa$).

The distal curvature is measured at the distal rib end rotational coordinate (θ_{end}). The posterior extension curvature is measured at the rib location furthest from a line drawn between the proximal rib end and the rib peak (at [X_{Pk}, Y_{Pk}]). This corresponds to a rotational coordinate (θ_{post}) for substitution in Eq. (1):

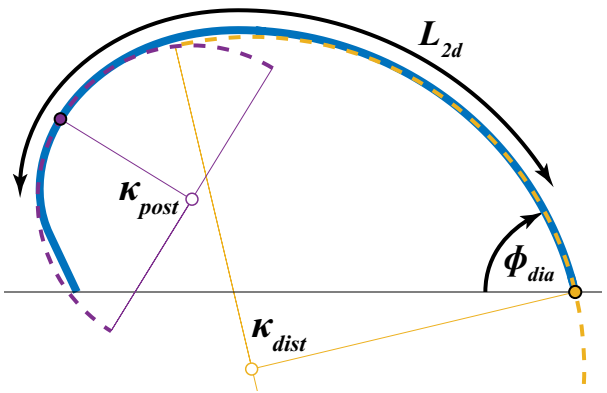

Fig. 4 Derived geometric shape measurements of arc length (L_{2d}, mm), distal inner angle (ϕ_{dia}, deg) and local curvature at the rib posterior and distal end locations (κ_{Post}, κ_{Dist}, mm^{-1}).

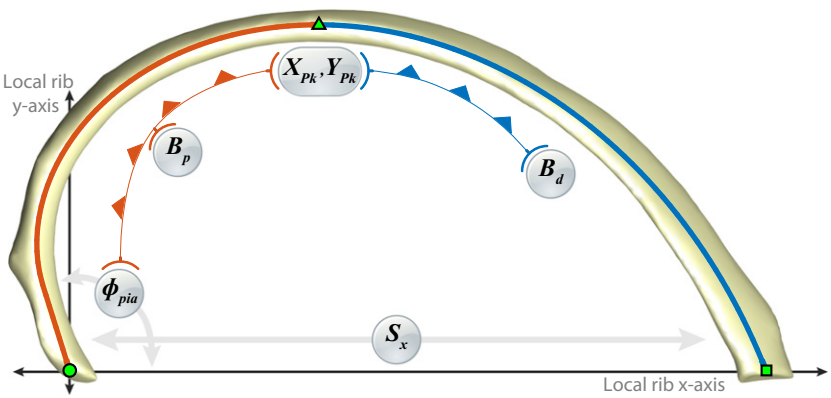

Fig. 3 Six-parameter rib model with one size (S_x) and five shape parameters. The proximal spiral (from circle to triangle markers) and distal spiral (from triangle to square markers) meet with zero slope at [X_{Pk}, Y_{Pk}] in normalized rib coordinates, defining rib aspect ratio (Y_{Pk}) and skewness (X_{Pk}). ϕ_{pia} defines the inner angle between the proximal rib end and the local *x*-axis, while B_p and B_d are proximal and distal spiral constants, respectively.

$$\theta_{post} = 2\arctan\left(\sqrt{B_P^2 + 1} + B_P\right) \quad (2)$$

Statistical analysis and methods

Data for this study are presented in two forms. First, scattered data plots showing the overall trends with age of each of the rib shape model parameters are given, and are accompanied by simple univariate regression results calculated separately for males and females showing the ability of age and sex alone to predict rib shape factors. Secondly, multivariable linear regression is performed, regressing the rib shape parameter values to the demographic factors of age, height, weight, and sex. Coefficients from the multivariable regression analyses quantify the independent effects of each demographic factor on rib shape parameters, and are then used to graphically depict the expected variation in rib shapes as these demographic factors change. In all analyses, statistical significance is determined at the $P < 0.01$ level.

Results

Rib shape fit and variation by level

The six-parameter rib shape model was fitted to 20 627 uninjured adult ribs. For in-plane model fitting, the mean absolute error (MAE) between the parameterized model and points on the original geometry was 0.40 mm. Parameter distribution patterns across the rib cage (see Fig. A1) matched closely those originally reported from a smaller population in Holcombe et al. (2016), and the reader is directed to that study for discussion of rib-level trends. The population-wide data for each of the rib shape parameters also followed normal distributions, typified by those shown for 6th ribs shown in Fig. A2, which also shows inter-parameter correlations, discussed further below.

Scatter data and trends with age

Overall population results for each of the six rib shape parameters are shown in Fig. 5 and for each of the three rib orientation parameters in Fig. 6. Fitted linear regression lines to age for males and females are shown on the plots for each rib level and parameter, and the explanatory power (r-squared) of age to explain population variation is included.

The first row of plots in Fig. 5 shows that there is indeed a significant trend in rib end-to-end span (S_x) with age, with both male and female rib ends tending to separate with increasing age ($P < 0.0001$ for all ribs 1–11). The slope for both sexes at the 6th rib level is approximately 2.5 mm/decade, with an *r*-squared value of 7% for females and 8% for males. The second row of scattered data in Fig. 5 shows that increasing age is correlated with a decrease in the Y_{Pk} parameter (i.e. increase in aspect ratio, $P < 0.0001$ for ribs 1–11). Age alone explains around 20% of the aspect ratio variation at mid-level ribs in females and 17% in males. Rib skewness (X_{Pk}) also shows strong trends with age for lower-level ribs ($P < 0.0001$ for ribs 6–11, $P > 0.01$ for ribs 1–4). As individuals age, rib skewness in these areas tends to increase, with age capable of explaining around 9% of the population variance in both sexes for the 7th rib level. Other rib shape parameters show only marginal univariate trends with age, with a slight increase at upper rib levels in ϕ_{pia} ($P < 0.001$ for ribs 1–8) and decrease in B_p ($P < 0.01$ for ribs 3–6).

Rib pump-handle α_{PH} angles are given in Fig. 6, with most ribs oriented between 40° (more vertically hanging, 'narrow-chested') and 80° (closer to horizontal, 'barrel-chested'). Age associations with α_{PH} are strongest for males; $P < 0.0001$ for all male ribs, $P < 0.01$ for female ribs 1–3 and $P < 0.001$ ribs 8–11; however, the rate of change (1.43° per decade for males at the 6th ribs, 0.43° for females) and the percentage of population variation explained by age alone (8% within males, none for females) are low.

The lateral swing α_{LS} parameter shows clear differences by rib level since different ribs extend closer to the sternum (α_{LS} near 20°) in ribs 2 and 3, and finish more laterally with each successive rib level. In general only minor univariate trends with age are seen, with increased age associated with slight increases in α_{LS} angle for lower ribs in males ($P < 0.01$, ribs 7–10). Similarly, small univariate aging effect is seen in bucket-handle α_{BH} angles, with age alone unable to explain more than 1% of the overall population variance within either sex ($P > 0.01$ for all except ribs 7 and 8).

Multivariable regression models

The univariate analyses shown in Figs 5 and 6 highlight clear trends in a number of the model parameters with age; however, they are not necessarily independent of confounding demographic variables such as height and weight, which will also affect rib geometry. Multivariable linear regression was therefore performed for each rib and parameter using demographic variables of age, height, weight, and sex as predictors. Full model regression coefficients for all parameters are supplied in Table A2, and Table 2 gives the proportion of population variation within each parameter that is explained by the demographics predictors in each regression model.

Regression results show, for example, that a person's height is the most strongly correlated demographic with rib end-to-end span (S_x), and that the 6th rib span increases at a rate of 0.54 mm for each gained cm in stature ($P < 0.0001$). Similarly, males will have a 6th rib S_x span 10.8 mm longer than females of equivalent demographics, and the isolated age effect on S_x is an elongation of 2.5 mm per decade ($P < 0.0001$).

Aspect ratio, on the other hand, is most strongly related to an increase with age, with the peak of the 6th rib (Y_{Pk}) moving down towards the *x*-axis in the local rib plane at a rate of 0.01 normalized rib units per decade ($P < 0.0001$). Sex and height have negligible influence on Y_{Pk} values for

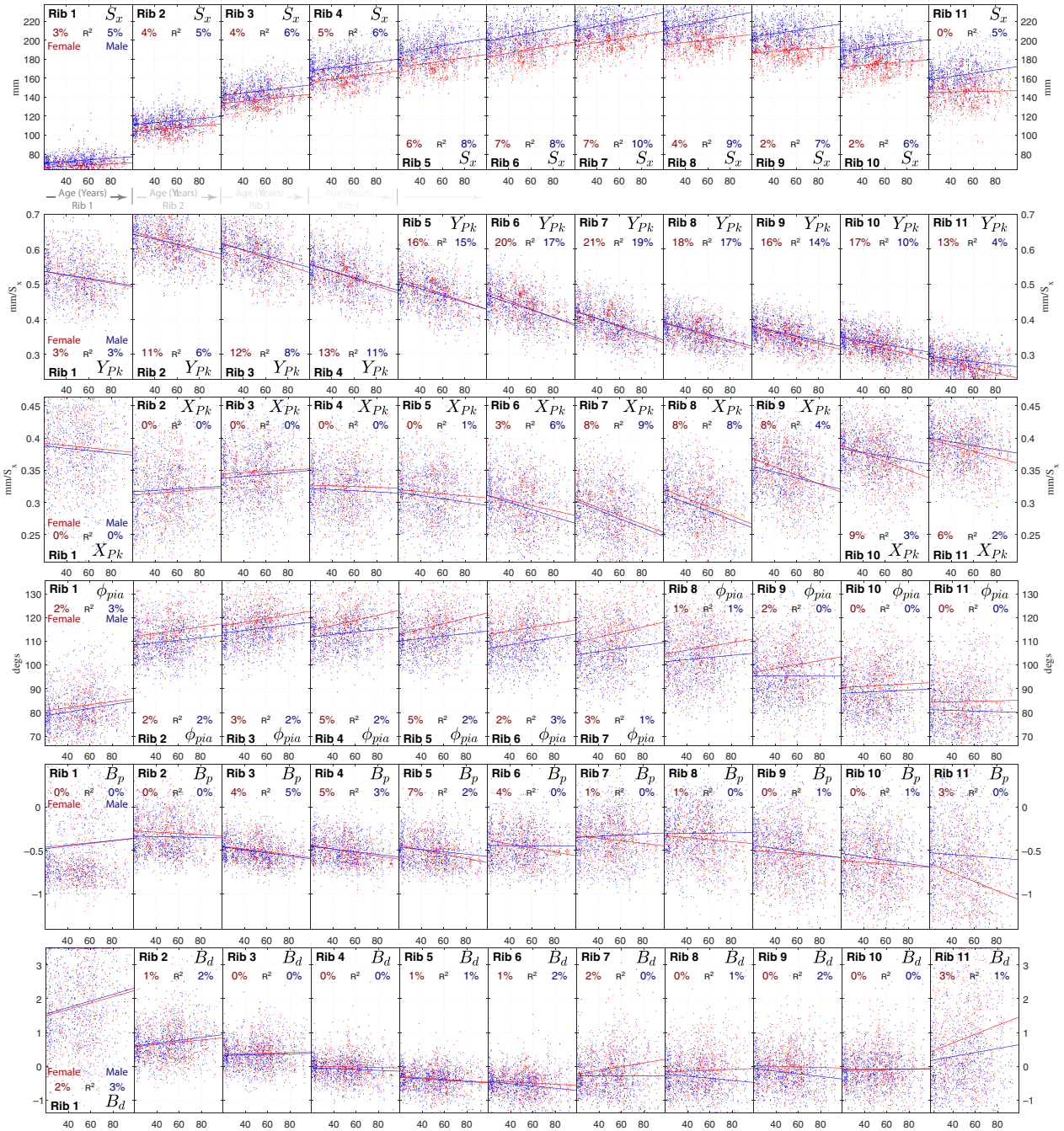

Fig. 5 Data point cloud showing all fitted in-plane parameters between ages 20 and 90 years for males (blue) and females (red). Linear regression lines are shown along with their explanatory power (*r*-squared). Strongest trends with age are seen for rib aspect ratio (Y_{Pk}), rib end-to-end length (S_x), and rib skewness (X_{Pk}) in mid- and lower-level ribs.

most ribs, whereas the independent effect of weight is to increase aspect ratio at a rate of 0.036 normalized rib units per 10 kg gained ($P < 0.0001$).

Rib skewness is primarily influenced by age and height, with a movement of the 6th rib X_{Pk} coordinate towards the proximal end by about 0.005 normalized rib units per decade and 0.0005 units per cm gained in stature ($P < 0.0001$). ϕ_{pia} differs significantly by sex, with female 6th ribs pointing initially 5.7° more posteriorly than male ribs, and a less strong independent age and weight effect also exists, whereby ribs increase in ϕ_{pia} by around 0.7° per decade and decrease by 0.6° per added 10 kg.

Using the full model parameters presented in Table A2, we can predict the expected set of six shape parameters per rib for a person of a known demographic, and with those parameters then generate that demographic's expected

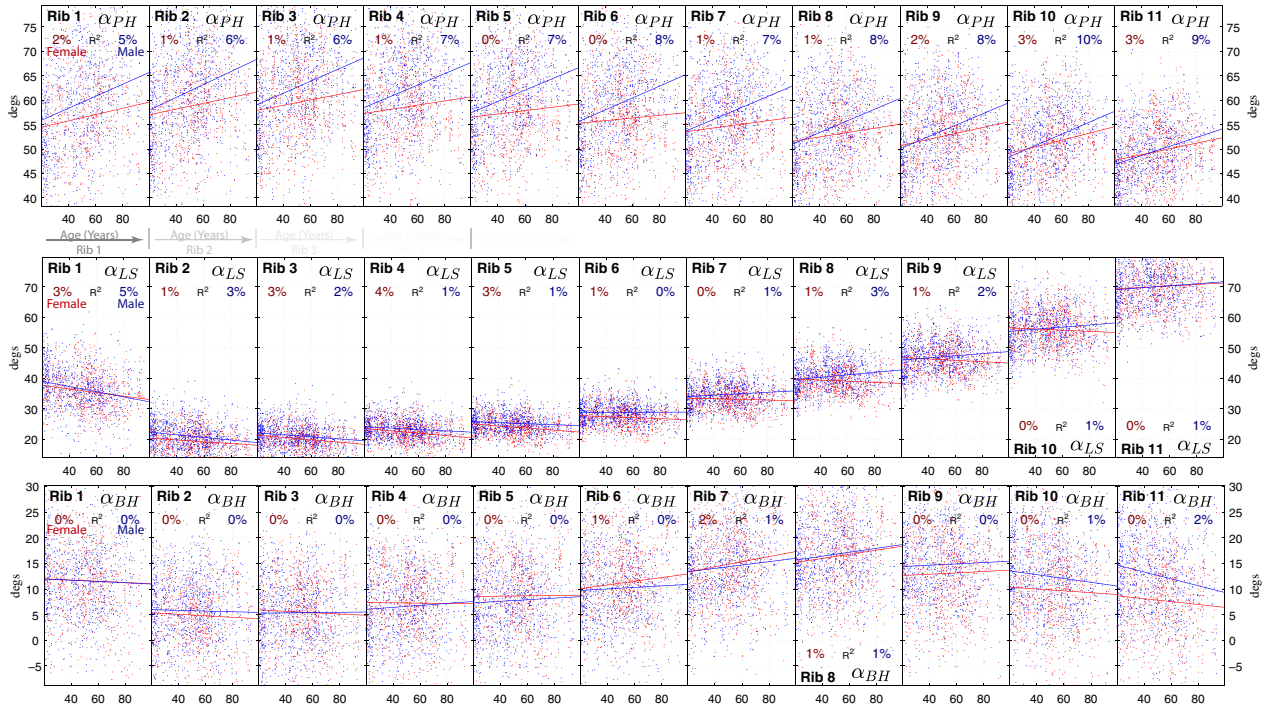

Fig. 6 Data point cloud showing all rib pump-handle (α_{PH}), lateral swing (α_{LS}), and bucket-handle (α_{BH}) angle parameters between ages 20 and 90 years for males (blue) and females (red). Linear regression lines are included along with their explanatory power (r-squared).

Table 2 Percentage of overall population variation per parameter explained (*r*-squared) by regression models to age, height, weight, sex.

No.	S_x	X_{Pk}	Y_{Pk}	ϕ_{pia}	B_p	B_d	α_{PH}	α_{LS}	α_{BH}
1	23	0	4	4	0	2	30	12	10
2	22	2	8	9	1	2	38	11	1
3	23	5	9	8	6	1	43	10	1
4	28	3	12	10	6	2	45	10	2
5	36	2	16	11	4	1	49	8	3
6	38	4	20	13	1	2	52	6	5
7	39	9	23	13	1	4	52	3	8
8	47	10	22	8	2	5	50	3	13
9	50	9	19	6	1	5	50	2	16
10	49	7	16	5	3	−0	48	3	17
11	35	7	14	3	8	5	41	2	17
12	12	4	4	1	1	0	7	2	8

geometric rib shapes. For example, Fig. 7 shows the expected geometric rib shapes determined by the regressed model parameters that are typical for three females and three males of 50 years of age with heights and weights equal to the CDC 5th, 50th, and 95th percentile height and weight for their respective sexes (see Table 1).

This same approach is used to illustrate the aging effect on rib shapes in Fig. 8. Here, just one stature demographic is held constant (50th percentile female), and person age is varied from 20 to 90 years at 5-year increments. From this figure it is clear to see the effect of elongation of the rib span (with the 6th rib S_x progressing from 179 to 197 mm) coupled with an increase in overall aspect ratio (Y_{Pk} shifting from 0.31 to 0.28 in normalized rib coordinates).

Similarly, Fig. 9 shows the expected change in rib shapes due to weight. A 50-year-old, 162-cm-tall female baseline is used, and weight is varied from 40 to 175 kg. The results show that rib shape changes primarily in the mid-to lower ribs, with expansion of the lateral rib aspects as weight is gained. The maximum physical separation between the expected rib shapes for the 40 and 175 kg individual in this figure occurs at the antero-lateral region of the 8th rib, where the rib paths differ by up to 9 mm in the local rib plane.

Testing model accuracy via indirect parameters

The results seen in Fig. 8 show the changes in rib shapes built from sets of shape model parameters that are themselves predicted by regressions to specific demographics (in this case a 50th percentile female of various ages). In that sense, all regressed parameters including the direct geometric measures of rib size (S_x), aspect ratio (Y_{Pk}), skewness X_{Pk}, and proximal inner angle (ϕ_{pia}) match the estimated central value for the supplied demographic, at least to the accuracy of the regression models.

However, this does not guarantee that any derived measures of shape (i.e. not explicitly regressed to as model

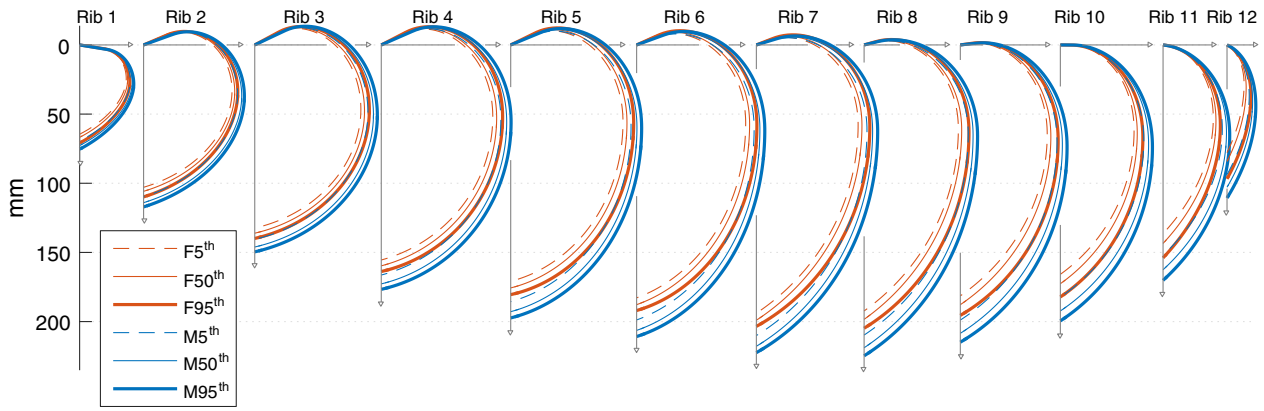

Fig. 7 Predicted in-plane rib shapes by demographic for small, medium, and large (CDC 5th, 50th, and 95th percentile weight and stature) males and females, all at 50 years of age.

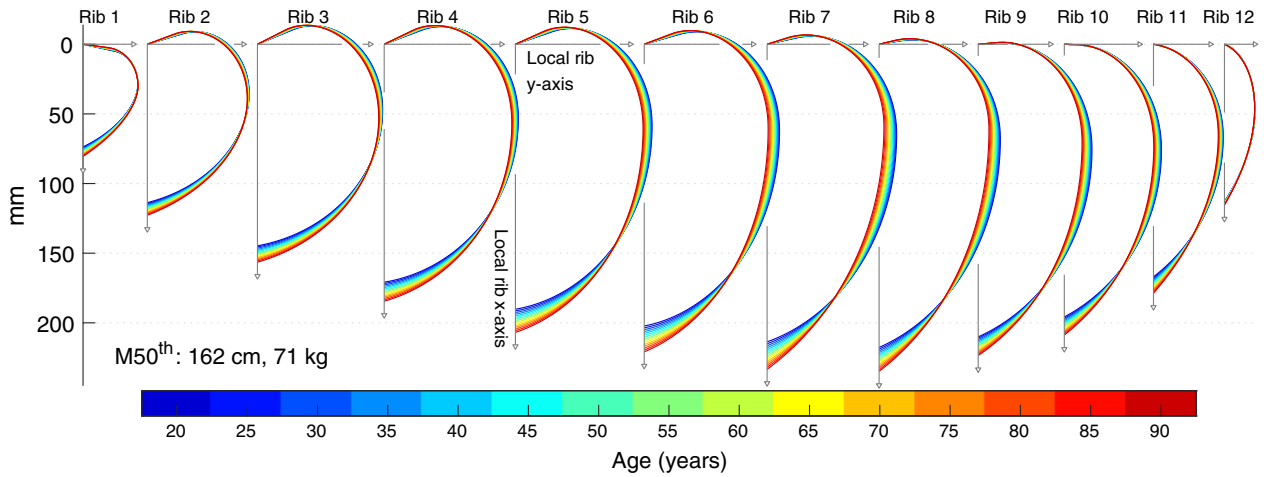

Fig. 8 Predicted in-plane rib shapes by age. Baseline demographic is the 50th percentile female with specific age represented by line color. Ribs become more elongated and increase in aspect ratio with age.

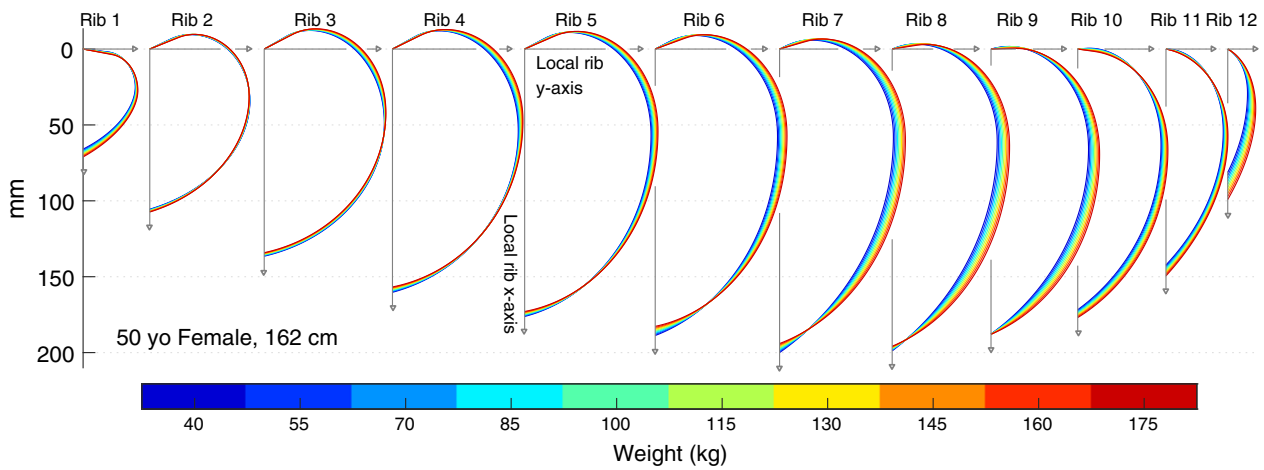

Fig. 9 Predicted in-plane rib shapes by weight. Baseline demographic is a 50-year-old female of 162 cm stature, with specific weight represented by line color. Ribs in heavier individuals are rounder, with a having lower aspect ratio (higher Y_{Pk}).

parameters) will also reflect the typical values for a given demographic. For example, the inner angle at the distal end (ϕ_{pia}) is one such rib shape measure which, when measured directly from all ribs in the population, is seen to decrease with age ($P < 0.001$ for all rib levels). The extent to which reconstructed rib shapes reflect such trends seen in indirect parameters–when using ribs that are rebuilt by sets of predicted parameters with different ages as input to regression–serves to test of the suitability of the model presented here to produce geometry that truly reflects overall population trends.

This comparison is illustrated in Fig. 10, which shows both expected values (via regression to demographics of the values measured directly from ribs in the population) and obtained values (via rebuilt ribs using predicted parameter values for that demographic) for each of the four indirect shape measures. The displayed demographic series is the 50th percentile female, with each observation matching one rib shape from the series of F50th ribs shown in Fig. 8. Corresponding figures for results from small and large female and male baseline demographics are given in Figs A3–A6.

Results in Fig. 10 show that the reconstructed ribs have an equivalent length (L_{2d}) to the expected rib length seen in the population. Trends in inner angle at the distal end (ϕ_{dia}) and rib curvature at the posterior region (κ_{Post}) also match well with the expected population values, with only marginally lower values in reconstructed ribs than expected based on measures from the given population. Rib curvature at the distal end shows some degree of divergence from population trends, with reconstructed ribs having around 10% lower curvature at this distal extremity than is expected, particularly at the 6th rib level in an older population.

Discussion

This study has applied parametric models of in-plane rib shape and rib orientation to a large collection of adult rib geometries to characterize the population variation and, in particular, investigate the changes in overall rib anatomy that occur with age. Multivariable (age, height, weight, sex) regression models for parameters show significant differences in size, shape, and orientation across demographics and are used to produce typical or expected rib shapes for particular demographics. The shape model and regression models are valuable tools for studying age-related anatomic changes and the associated injuries which may be affected by overall rib and rib cage geometry.

Rib shape model considerations

A feature of the shape model introduced in Holcombe et al. (2016) and used here, is that four of its six parameters are themselves inherent geometric measures of rib geometry. This provides an advantage over other generalized methods of rib cage shape analysis such as GPA or PCA – which parameterize the position of a large cloud of points – by ensuring that the shape model's regression coefficients for demographic factors are themselves directly meaningful and easily understood. For example, the negative coefficients for age in the Y_{Pk} parameter of Table A2 give clear evidence of increasing aspect ratios in ribs throughout adulthood. The shape model also provides a more concise set of parameters than would otherwise be obtained using point cloud data, and results in Fig. A2 show that these parameters are each normally distributed across the population, lending validity to subsequent regression analyses. It should be noted, however, that most of the inter-parameter correlations from Fig. A2 are statistically significant ($P < 0.01$). The strongest geometric correlations are between S_x and Y_{Pk} (Pearson's $R = 0.64$) and Y_{Pk} and X_{Pk} ($R = 0.43$), showing that ribs with higher aspect ratio (designated by lower Y_{Pk}) tend to be longer and also have their peak slightly shifted towards the middle of the rib (lower skewness). Overall, these correlations indicate that – statistically speaking – there might be ways to parameterize rib shapes that are even more efficient than our chosen six-parameter model, albeit likely at the expense of using parameters with intrinsic geometric meaning.

Another important aspect of the shape model is its accuracy in representing the underlying geometric rib data. The mean absolute error (MAE) between a target rib point and its fitted shape model was 0.40 mm. For comparison with past literature, Kindig's seven-parameter geometric model based on a circle and a semi-ellipse$_{20}$ reported an MAE of 0.78 mm, indicating that, on average, the spiral model used here offers an over 40% reduction in geometric fitting error.

Measures of curvature using the shape model from this study showed strong agreement with previously published results. Mohr et al. (2007) reported an average curvature of 0.017 mm^{-1} at the posterior regions of mid-level ribs and Dansereau & Stokes (1988) reported a maximum curvature along the whole rib between 0.018 and 0.033 mm^{-1}. In this study the average κ_{Post} values for ribs 3–9 fell between 0.017 and 0.021 mm^{-1}. At the distal end of the ribs, average κ_{Dist} values in this study ranged from 0.007 to 0.011 mm^{-1}, which is similar to the range of 0.006 to 0.008 mm^{-1} reported by Mohr et al. (2007).

Rib changes by demographics

This study attempts to identify specific effects of age on overall rib shape and orientation. Increases in rib pump-handle α_{PH} angle were first noted as both a weight effect and an aging effect in males by Kent et al. (2005). This age effect has since been confirmed by multiple studies (Gayzik et al. 2008; Shi et al. 2014; Weaver et al. 2014; Wang et al. 2016), albeit with age capable of explaining a relatively low proportion of the overall population variation in rib angle

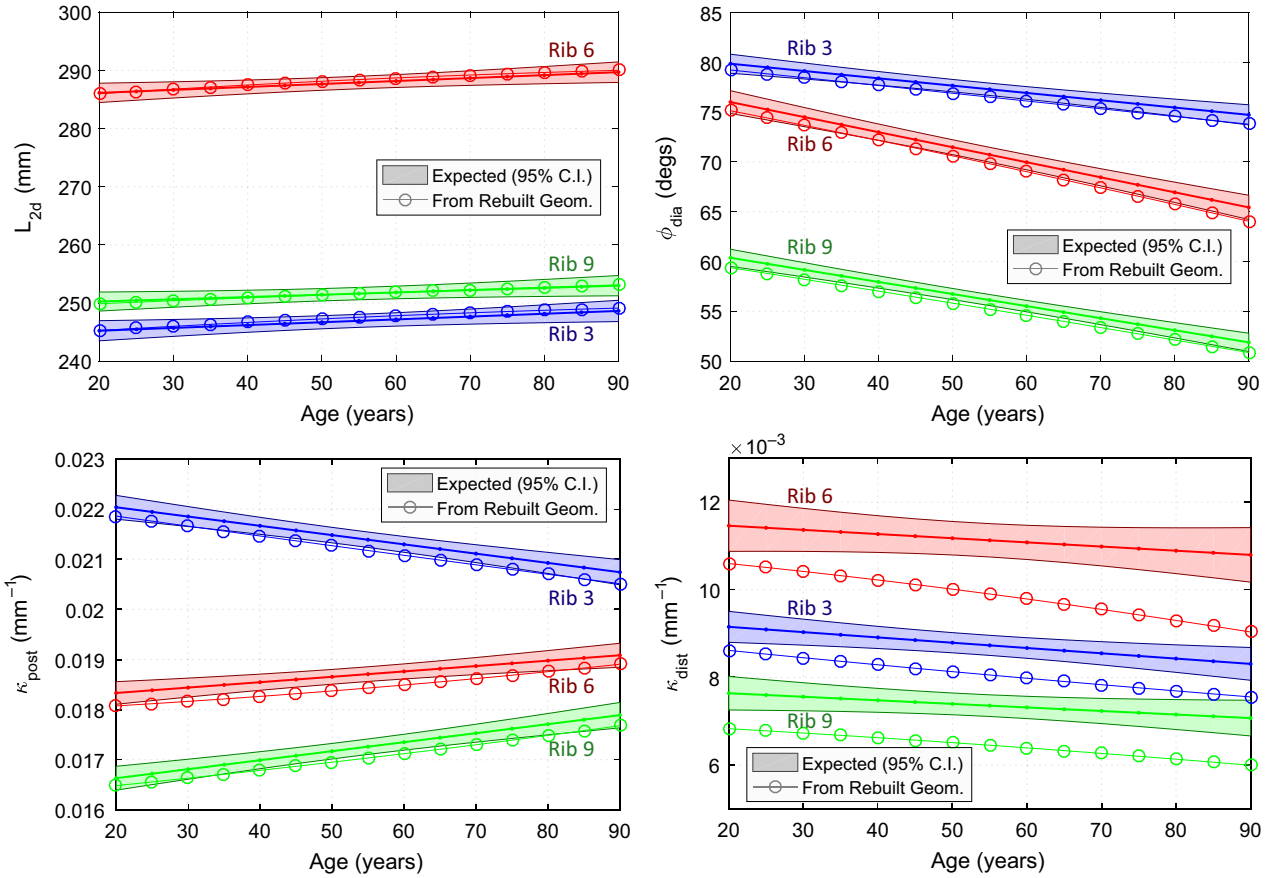

Fig. 10 Expected values for rib arc length (L_{2d}), inner angle at the distal end (ϕ_{dia}), and local curvature at posterior (κ_{Post}) and distal (κ_{Dist}) locations, along with values from rebuilt ribs matching that demographic. Regression models fitted to the values measured directly in the population are used to determine the expected values (with 95% confidence interval) for 50th percentile females of varying ages.

(4% and 7% as reported for males by Kent et al. (2005) and Weaver et al. (2014), respectively, and with methodology differing across studies). Here we show similar results, with a positive correlation found between age alone and α_{PH} capable of explaining 8% of male variability and 1% ($P < 0.001$) of female variability at mid-level ribs. Our multivariable results show that the inclusion of weight substantially increases this predictive power (*r*-squared up to 50% for mid-level ribs) reflecting results from Kent et al. (2005) whereby weight alone was found to better predict rib angle than age did (*r*-squared equal to 36%). These results suggest obesity (or weight gain in general) is strongly related to the physical rotation of ribs towards a more horizontal configuration, possibly to accommodate greater volumes of fat and other soft tissues within the chest and abdominal cavity. Similarly, results also show an independent sex effect whereby α_{PH} rib angles in males are seen to be around 3° more horizontal than in females of equivalent demographics. A reason for this sex difference may come from the differences in typical body fat patterns, whereby fat accumulation in males tends to produce relatively higher proportions of visceral fat (resulting in outward pressure from the abdomen and chest), whereas females tend to accumulate higher proportions of subcutaneous fat (which is outside the rib cage and less likely to affect rib angles) (Enzi et al. 1986).

Beyond results for rib angle, however, a more direct aging effect is highlighted in Fig. 8, whereby older ribs elongate in end-to-end span and adopt a shallower overall curvature; these changes are reflected in the age coefficients for the S_x and Y_{Pk} parameters of Table A2. The independent effect of age is to increase rib S_x span by up to 2.7 mm (7th rib, $P < 0.001$ for ribs 1–10) for every added decade. As a result, across a 70-year adult lifetime an individual of average stature is likely to see the separation between ends of their longest ribs expand by 2.7 cm, or approximately 13%. This elongation is coupled with increases in rib aspect ratio, with Y_{Pk} being significantly associated with age for ribs 1–11 ($P < 0.001$ in ribs 1–10). The result of this association is that the rib peak moves progressively closer to the *x*-axis of the local rib plane at a rate of between 0.006 (ribs 1 and 10) and 0.01 (mid-level ribs) normalized rib units per decade. For perspective on these primary aging effects, a 70-year age difference reflects 6th

rib changes in Y_{Pk} that amount to 1.5 SD from population distributions in Y_{Pk}, and changes in S_x that amount to 1.1 SD from population distributions in S_x. Each of these shape effects is more strongly associated with age than the 0.8 SD changes seen in α_{PH}.

Other independent associations with age tend to be less strong and affect a more limited region of the rib cage. For instance, an age effect on rib skewness is most prominent at mid- to lower level ribs (reductions in X_{Pk} of between 0.002 and 0.007 units per decade), whereas age influences ϕ_{pia} angle more prominently in mid- to upper level ribs (increasing by around 0.7° per decade). In the case of ϕ_{pia} there is also a clear sex effect, with females having higher ϕ_{pia} angles than males of equivalent demographics by up to 6.3° ($P < 0.001$). Sex is most prominently different in overall rib size, with S_x seen to be between 2.5 mm (1th rib) and 10.9 mm (8th rib) longer in males than females of equivalent demographics. Although these sex differences occur independently of other demographics and indicate subtle underlying differences between female and male rib cage morphology, it should also be recognized that the magnitudes of these differences are small compared with individual variability shown for the S_x and ϕ_{pia} parameters. Person height is also strongly correlated with S_x, with each additional 1 cm in stature corresponding to 0.2–0.6 mm extension of S_x at each rib ($P < 0.001$). Weight is the only demographic variable other than age that is independently associated with aspect ratio, in which a small increase is seen in Y_{Pk} for ribs 4–10 of 0.001–0.004 normalized rib units per each added 10 kg. Such changes are consistent with the accumulation of body fat within the thorax resulting in increased outward pressure to the rib cage. In general there are few consistent trends across series of rib levels when considering the B_p and B_d spiral constants. Only in B_d do we see decreasing values for ribs 2–11; however, these do not reach statistical significance ($0.03 < P < 0.05$ for ribs 3–6 and 9–11).

Overall, each of the differences that are seen in Table A2 has an accumulated effect to influence rib shape in multiple ways across demographics as depicted by Figs 7–9. It is important to consider that each of these figures shows only the typical, or statistically central, geometry for each specific demographic, whereas the constituent population itself contains rib geometries exhibiting a much wider range of individuality. This is reflected by the degree of scatter seen in Fig. 5, and by the fact that the explanatory power (r-squared) of demographics alone to predict rib shape parameters remains below 0.2 for most shape parameters. The particular aging effect of elongation coupled with increased aspect ratio is consistent with Shi et al. (2014) and Wang et al. (2016), who reported an increase in the whole rib cage AP depth with age that was associated with a decrease in rib cage width especially in the middle of the rib cage. To the best of our knowledge this is the first study to directly identify these effects as shape changes to the ribs that are independent of other thoracic changes, and the first to quantify both the shape changes themselves and the ability of demographics-based regression to represent the overall population variability.

Potential mechanisms for age-related shape changes

The results for changing rib shape with age were associated ($P < 0.001$) with an in-plane increase in rib arc length (L_{2d}) as seen in Fig. 10. However, when considering the entire rib centroidal length including out-of-plane deviation (L_{3d}), this association with age was no longer present ($P > 0.4$). These results indicate that the shape changes identified here do not serve to alter the overall bone length with age, but merely adjust over time the path that is taken from its proximal to distal end. Although it is not the focus of this paper to investigate the underlying mechanisms that bring about this change, a number of potential causes can be identified.

First, increased osteoporosis is a well-documented aging phenomena and, in the spine, this reduction in bone mineral content leads to deterioration of vertebral support and an associated increase in kyphotic spine curvature over time. Osteoporotic bone loss also occurs in ribs and is observed in the form of a progressive decrease in cortical area with age (Pavón et al. 2010) and an associated increase in intracortical porosity (Agnew & Stout, 2012). With the complex distribution of material properties and cortical thicknesses across a rib's surface (Kemper et al. 2007), degradation of bone materials may lead to altered stress states within the ribs which could serve to gradually modify their overall geometric makeup. Given the more advanced rates of osteoporosis seen in women than in men (Cawthon, 2011), one might expect that changes in rib shapes due primarily to the effects of osteoporosis would be similarly accelerated in females compared with males. This hypothesis was tested by the addition of an interaction term between age and sex to the multivariable regression models for the two primary rib shape parameters associated with age (S_x, Y_{Pk}). The additional interaction term was not significantly different to zero ($P > 0.01$) for any mid-level ribs and parameters, including those shown to be most strongly associated with age (S_x, Y_{Pk}). In other words, the age effects on rib shape identified in this study were not found to be significantly different between males and females, casting doubt on the hypothesis that rib shape changes might come solely from the effects of osteoporosis.

Another hypothesis comes from an increase in calcification of the costal cartilage that is known to occur with age (Navani et al. 1970; Semine & Damon, 1975; Stewart & McCormick, 1984). Ribs are connected to the sternum via direct costal cartilage segments (true ribs 1–5) or indirectly via segments attached to superior cartilage segments (false ribs 6–10), and the presence of calcification is known to increase the local material and cartilage segment stiffness (Guo et al. 2007; Lau et al. 2015). As the compliance of the

chest is reduced due to calcification of these costal segments, the internal stresses experienced by the connecting ribs are likely to change, producing a possible mechanism for changes in overall rib shapes. Similarly, changes over time to musculature surrounding or attached to the ribs may provide a mechanism for altering rib geometry. Sarcopenia (loss of muscle mass) is a well known age-related phenomenon affecting skeletal muscle, and is also likely to be present in respiratory musculature such as the intercostal muscles and diaphragm (Tolep & Kelsen, 1993). This weakening over time of these tissues that offer structural support to the ribs has the potential to in turn lead to gradual changes in rib bone shape.

Limitations

The resolution of the CT scans used in any medical imaging study poses a limitation on accuracy when extracting underlying geometry. For instance, Perz et al. (2015) showed that simple thresholding of bone in cross-sectional views produced significant error when measuring cortical bone cross-sectional area in lower resolution clinical CT scans. The shape model investigated here focuses only on the central axis of the rib and does not attempt to capture cross-sectional geometry or other changes in rib cortical surfaces that may vary across the population. This is itself a limitation in terms of the results that are reported in this study; however, it also serves to alleviate problems with scan resolution since overall rib cross-sections (from which the central axis is derived) are structures many times larger than pixel sizes in even the lowest resolution scans. A sensitivity analysis (provided as Appendix S1) across the full range of scan resolutions and slice spacing found that the error in absolute position of any given cross-sectional data point in lower resolution scans was 0.36 (+0.19) mm, whereas the resulting error in geometric shape model parameters such as size and aspect ratio was below 0.4%.

The population itself is large compared with previous studies of rib and rib cage shape, with data from 1042 live subjects. While study demographics match well to the general US population, it should be noted that subjects are sampled from one region of North America and individual ethnicity was not considered, so care should be taken when extending results to different regional populations.

The CT scans were taken under a trauma protocol having the patients hold their breath during the image capturing sequence, meaning results reported here are for a condition of maximal lung inspiration. It is expected that some patients may have had difficulty adhering to this protocol, particularly those with chest injuries, and this could lead to variations in measured rib angle from an otherwise healthy population due to expected differences throughout a respiratory cycle (Bellemare et al. 2001, 2003).

Rib pump-handle α_{PH} angles are reported with respect to the scan coronal plane or scanning bed. However, spine posture varies throughout the population, and since ribs articulate directly with the spine, kyphosis seen in some portions of the elderly population (Bartynski et al. 2005) would serve to lower α_{PH} angles in those individuals. This difference should be accounted for when comparing the current results with measures of independent orientation of ribs with respect to a curved spine rather than a fixed reference plane.

The inner organs and other internal anatomy of the chest are asymmetrical, which would in turn lead to some degree of asymmetry between left- and right-sided rib anatomy. Small but statistically significant differences in X_{Pk} and ϕ_{pia} parameters across sides were observed, indicating some nominal difference in skewness between ribs on the left and right sides of the body. With the goal of this study being to describe the more substantial variations seen across demographics, however, ribs from left and right sides were pooled and results reported by rib level only.

Finally, results show that some amount of care should be taken when using the demographics-based regression model in applications that are strongly dependent on the local curvature at the distal end of the rib (κ_{dist}). The regression models for each direct parameter (size, aspect ratio, skewness, inner angle at the proximal end) ensure a central estimate is obtained for a given demographic, and results also show that indirect measures of rib length, distal inner angle, and posterior rib curvature are very well represented when recreating ribs from these regressed parameters. However, the indirect property of distal rib curvature (κ_{dist}) is seen to be slightly underestimated in these recreated rib shapes when compared with true curvature seen directly in the population.

Future work and applications

Key components that drive the biomechanical response of ribs to loading include cross-sectional and cortical geometry, as well as the out-of-plane deviation of the rib's centroidal path. A natural extension of the six-parameter in-plane shape model is to expand parameterization to these components, and – provided that appropriate data sources are used that can accurately resolve these finer details – apply such measurement to a broad population. Future work could then quantify the relative influence of age on the individual geometric and material components in human ribs and provide necessary data for age-specific models of thoracic anatomy. Results from this study also have relevance in a number of clinical settings. Data presented here provide normal quantitative ranges for rib shape that are seen throughout the adult population, and the associations between those parameters and lung capacity or other measures of disease state may produce clinically meaningful metrics in the diagnosis and treatment of thoracic skeleton defects and respiratory disease.

Conclusions

A statistical model of the human rib shape and orientation in the body was developed that accounts for variations by age, height, weight, and sex. The size and shape of ribs were represented using a six-parameter shape model which was applied to 1042 subjects, and multivariable regression was used for a predictive model of typical rib geometry based on demographic factors. All demographic factors had statistically significant effects on rib shape and orientation, with height and sex being most strongly associated with rib size, and weight being most strongly associated with rib pump-handle angle. The primary effect of age was on a unique aspect of rib shape, with older ribs being more elongated and having flatter overall curvature than younger ribs. Study results include a statistical rib shape model that gives the geometric basis for building ribs that are typical for any specific demographics group, which can in turn be used to enhance computational modeling of the thoracic rib cage for injury prevention and, in particular, provide a quantitative basis for changing rib shapes by age.

Conflict of interest

The authors have no conflict of interest that could influence the work described in this manuscript.

References

Agnew AM, Stout SD (2012) Brief communication: reevaluating osteoporosis in human ribs: the role of intracortical porosity. *Am J Phys Anthropol* **148**, 462–466.

Agnew AM, Schafman M, Moorhouse K, et al. (2015) The effect of age on the structural properties of human ribs. *J Mech Behav Biomed Mater* **41**, 302–314.

Bartynski WS, Heller MT, Grahovac SZ, et al. (2005) Severe thoracic kyphosis in the older patient in the absence of vertebral fracture: association of extreme curve with age. *Am J Neuroradiol* **26**, 2077–2085.

Bellemare J-F, Cordeau M-P, Leblanc P, et al. (2001) Thoracic dimensions at maximum lung inflation in normal subjects and in patients with obstructive and restrictive lung diseases. *Chest* **119**, 376–386.

Bellemare F, Jeanneret A, Couture J (2003) Sex differences in thoracic dimensions and configuration. *Am J Respir Crit Care Med* **168**, 305–312.

Bonne S, Schuerer DJE (2013) Trauma in the older adult. *Clin Geriatr Med* **29**, 137–150.

Cawthon PM (2011) Gender differences in osteoporosis and fractures. *Clin Orthop Relat Res* **469**, 1900–1905.

Dansereau J, Stokes IAF (1988) Measurements of the three-dimensional shape of the rib cage. *J Biomech* **21**, 893–901.

Enzi G, Gasparo M, Biondetti PR, et al. (1986) Subcutaneous and visceral fat distribution according to sex, age, and overweight, evaluated by computed tomography. *Am J Clin Nutr* **44**, 739–746.

Fryar CD, Gu Q, Ogden CL (2012) Anthropometric reference data for children and adults: United States, 2007–2010. Vital and Health Statistics. Series 11, Data from the National Health Survey. 1–48.

Galan G, Penalver J, Paris F, et al. (1992) Blunt chest injuries in 1696 patients. *Eur J Cardiothorac Surg* **6**, 284–287.

Gayzik FS, Yu MM, Danelson KA, et al. (2008) Quantification of age-related shape change of the human rib cage through geometric morphometrics. *J Biomech* **41**, 1545–1554.

Guo B-Y, Liao D-H, Li X-Y, et al. (2007) Age and gender related changes in biomechanical properties of healthy human costal cartilage. *Clin Biomech* **22**, 292–297.

Holcombe S, Kindig M, Zhang P, et al. (2014) Age-based predictive model of the pediatric ribcage. *Int J Autom Eng* **5**, 5–22.

Holcombe SA, Wang SC, Grotberg JB (2016) Modeling female and male rib geometry with logarithmic spirals. *J Biomech* **49**, 2995–3003.

Hu J, Reed MP (2012) Focusing on vulnerable populations in crashes: recent advances in finite element human models for injury biomechanics research. *J Autom Saf Ener* **3**, 295.

Kemper AR, McNally C, Pullins CA, et al. (2007) The biomechanics of human ribs: material and structural properties from dynamic tension and bending tests. *Stapp Car Crash J* **51**, 235–273.

Kent RW, Crandall JR, Bolton J, et al. (2001) The influence of superficial soft tissues and restraint condition on thoracic skeletal injury prediction. *Stapp Car Crash J* **45**, 183–204.

Kent R, Lee S-HH, Darvish K, et al. (2005) Structural and material changes in the aging thorax and their role in crash protection for older occupants. *Stapp Car Crash J* **49**, 231–249.

Kent R, Woods W, Bostrom O (2008) Fatality risk and the presence of rib fractures. *Annu Proc Assoc Adv Autom Med* **52**, 73–82.

Kindig MW, Kent RW (2013) Characterization of the centroidal geometry of human ribs. *J Biomech Eng* **135**, 11007.

Lau AG, Kindig MW, Salzar RS, et al. (2015) Micromechanical modeling of calcifying human costal cartilage using the generalized method of cells. *Acta Biomater* **18**, 226–235.

Lee WY, Yee WY, Cameron PA, et al. (2006) Road traffic injuries in the elderly. *Emerg Med J* **23**, 42–46.

Margulies SS, Rodarte JR, Hoffman EA (1989) Geometry and kinematics of dog ribs. *J Appl Physiol* **67**, 707–712.

Mohr M, Abrams E, Engel C, et al. (2007) Geometry of human ribs pertinent to orthopedic chest-wall reconstruction. *J Biomech* **40**, 1310–1317.

Navani S, Shah JR, Levy PS (1970) Determination of sex by costal cartilage calcification. *Am J Roentgenol* **108**, 771–774.

Pavón MV, Cucina A, Tiesler V (2010) New formulas to estimate age at death in maya populations using histomorphological changes in the fourth human rib. *J Forensic Sci* **55**, 473–477.

Perz R, Toczyski J, Subit D (2015) Variation in the human ribs geometrical properties and mechanical response based on X-ray computed tomography images resolution. *J Mech Behav Biomed Mater* **41**, 292–301.

Roberts SB (1977) Simple quantitative anatomical model for in-vivo human ribs. *J Bioeng* **1**, 443–453.

Roberts SB, Chen PH (1972) Global geometric characteristics of typical human ribs. *J Biomech* **5**, 191–201.

Schultz AB, Benson DR, Hirsch C (1974) Force-deformation properties of human ribs. *J Biomech* **7**, 303–309.

Semine AA, Damon A (1975) Costochondral ossification and aging in five populations. *Hum Biol* **47**, 101–116.

Shi X, Cao L, Reed MP, et al. (2014) A statistical human rib cage geometry model accounting for variations by age,

sex, stature and body mass index. *J Biomech* **47**, 2277–2285.

Slice DE, Stitzel J (2004) Landmark-based geometric morphometrics and the study of allometry. Proceedings of the Society of Automotive Engineers Digital Human Modeling for Design and Engineering Symposium, 199–207.

Söderlund T, Ikonen A, Pyhältö T, et al. (2015) Factors associated with in-hospital outcomes in 594 consecutive patients suffering from severe blunt chest trauma. *Scand J Surg* **104**, 115–120.

Staal J, van Ginneken B, Viergever MA (2007) Automatic rib segmentation and labeling in computed tomography scans using a general framework for detection, recognition and segmentation of objects in volumetric data. *Med Image Anal* **11**, 35–46.

Stewart JH, McCormick WF (1984) A sex- and age-limited ossification pattern in human costal cartilages. *Am J Clin Pathol* **81**, 765–769.

Tolep K, Kelsen SG (1993) Effect of aging on respiratory skeletal muscles. *Clin Chest Med* **14**, 363–378.

Veysi V, Nikolaou V, Paliobeis C, et al. (2009) Prevalence of chest trauma, associated injuries and mortality: a level I trauma centre experience. *Int Orthop* **33**, 1425–1433.

Wang Y, Cao L, Bai Z, et al. (2016) A parametric ribcage geometry model accounting for variations among the adult population. *J Biomech* **49**, 2791–2798.

Weaver AA, Schoell SL, Stitzel JD (2014) Morphometric analysis of variation in the ribs with age and sex. *J Anat* **225**, 246–261.

Weisstein EW (2016) Logarithmic Spiral. From MathWorld - A Wolfram Web Resource. http://mathworld.wolfram.com/LogarithmicSpiral.html, (accessed 4 April 2016).

Wuermser L-A, Achenbach SJ, Amin S, et al. (2011) What accounts for rib fractures in older adults? *J Osteoporos* **2011**, 1–6.

Supporting Information

Additional Supporting Information may be found in the online version of this article:

Appendix S1 Simulated scan resolutions.

Appendix

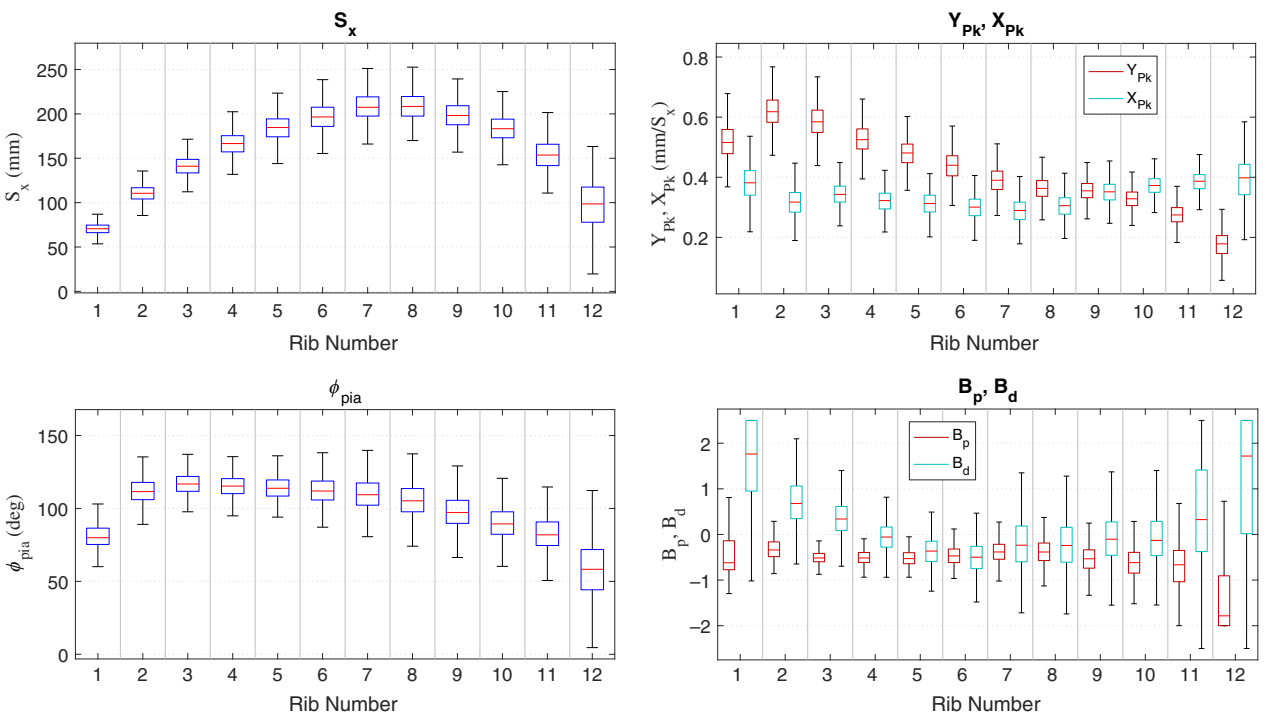

Fig. A1 The overall trends in in-plane model parameters across the adult population (n = 20 627 ribs). Boxes show the median and the 25th to 75th quantile ranges and whiskers extend to the $\pm$ 2.7σ range (99.7% coverage).

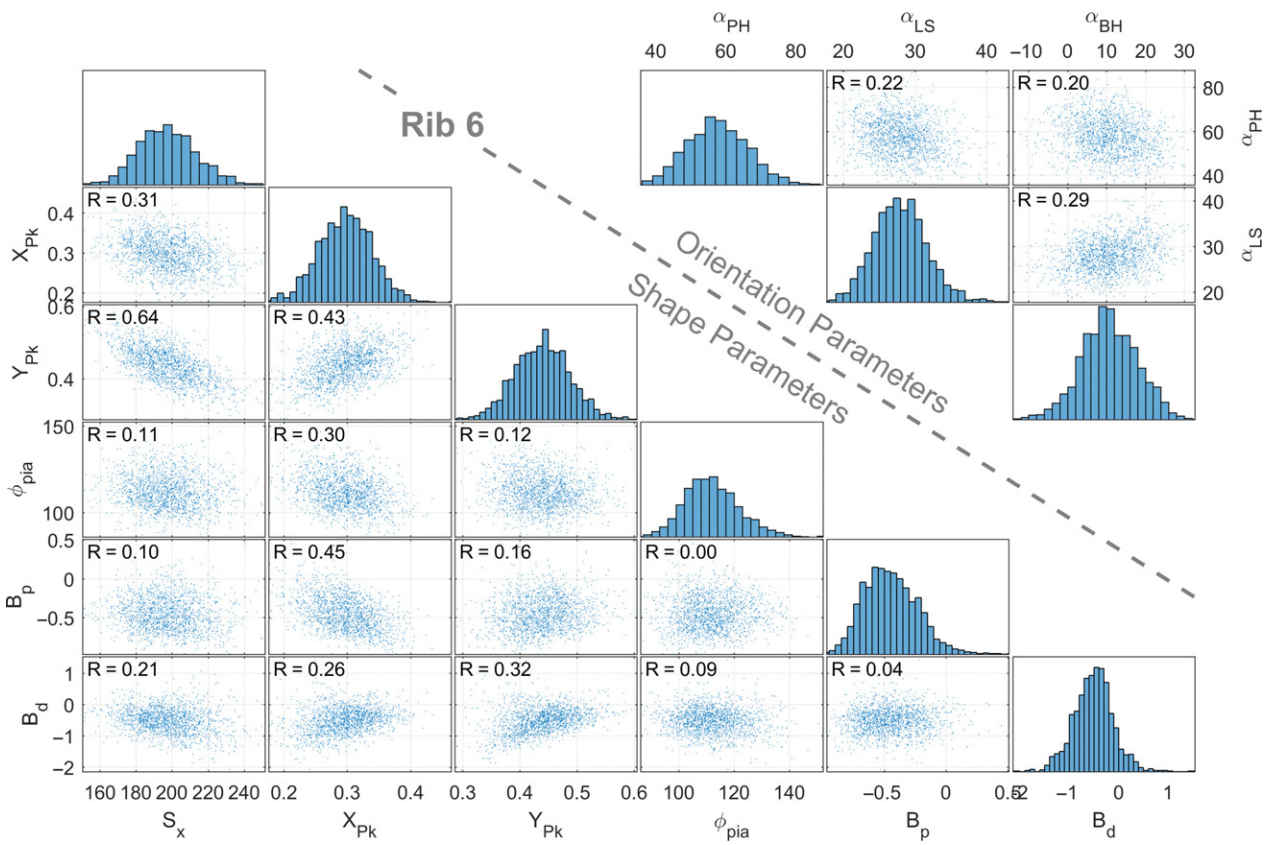

Fig. A2 Individual parameter histograms (main diagonal) and inter-parameter correlation plots for the 6th ribs. Histograms show parameter distributions in the population to be largely normal. While statistically significant for all pairs except B_p vs. ϕ_{pia} and B_p vs. B_d, inter-parameter correlations (Pearson's R) are low for most parameter combinations, with the strongest between rib size (S_x) and aspect ratio (Y_{Pk}).

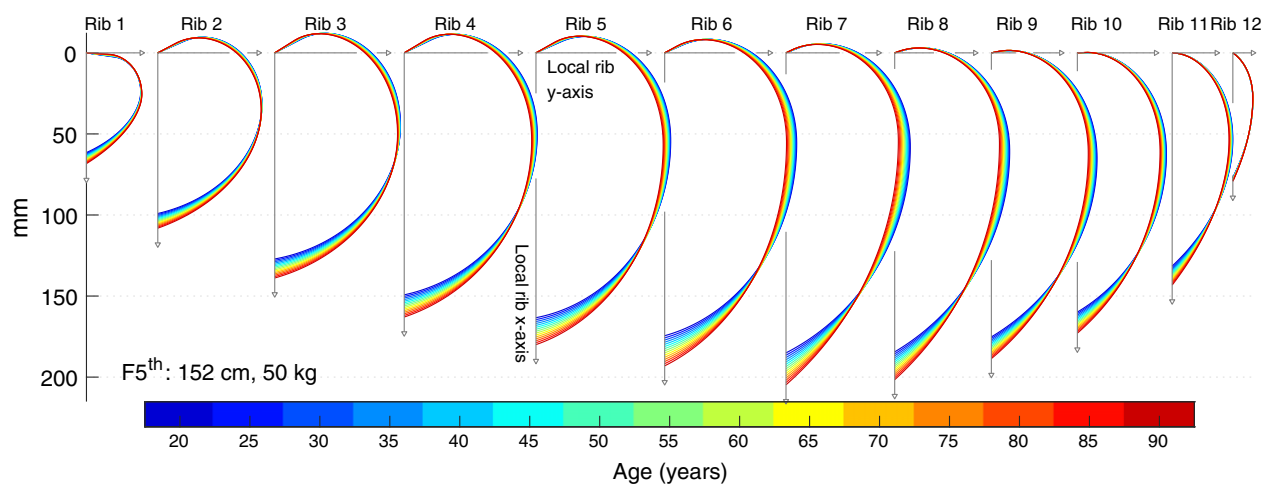

Fig. A3 Predicted in-plane rib shapes by age. Baseline demographic is the 5th percentile female with specific age represented by line color. Ribs become more elongated and increase in aspect ratio with age.

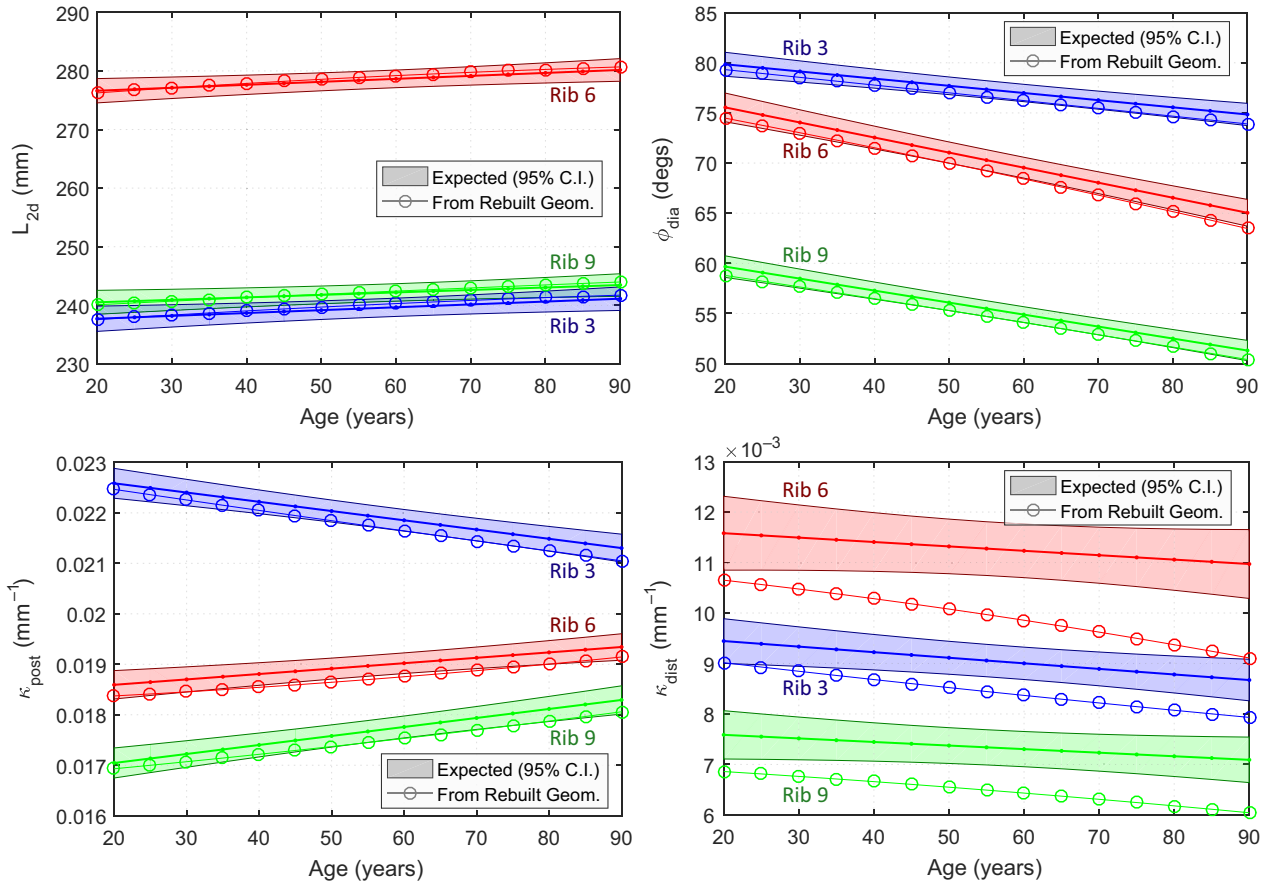

Fig. A4 Expected values for rib arc length (L_{2d}), inner angle at the distal end (ϕ_{dia}), and local curvature at posterior (κ_{Post}) and distal (κ_{Dist}) locations, along with values from rebuilt ribs matching that demographic. Regression models fitted to the values measured directly in the population are used to query for the expected values (with 95% confidence interval) for 5th percentile females of varying ages.

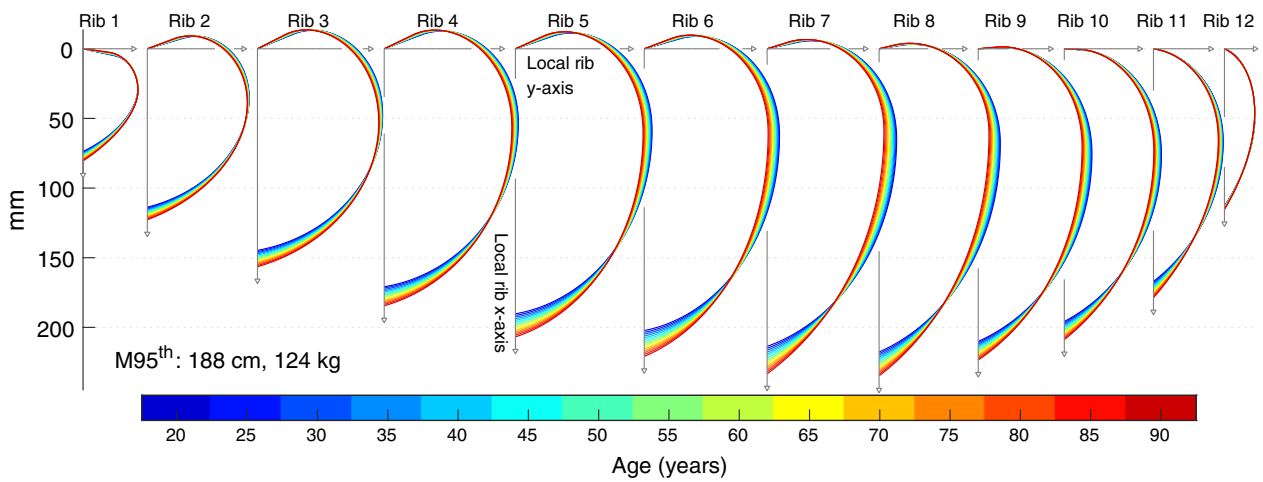

Fig. A5 Predicted in-plane rib shapes by age. Baseline demographic is the 95th percentile male with specific age represented by line color. Ribs become more elongated and increase in aspect ratio with age.

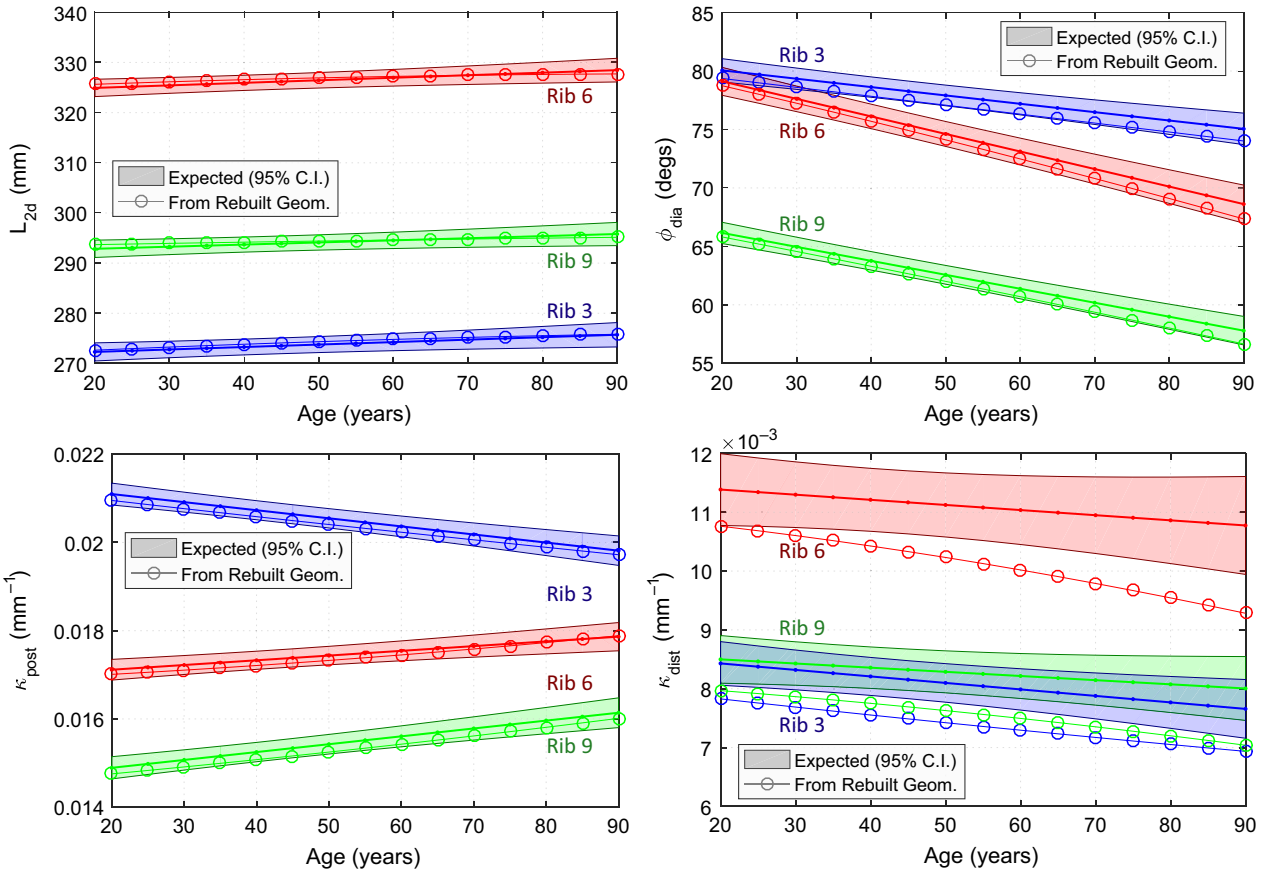

Fig. A6 Expected values for rib arc length (L_{2d}), inner angle at the distal end (ϕ_{dia}), and local curvature at posterior (κ_{Post}) and distal (κ_{Dist}) locations, along with values from rebuilt ribs matching that demographic. Regression models fitted to the values measured directly in the population are used to query for the expected values (with 95% confidence interval) for 95th percentile males of varying ages.

Table A1 Average ± standard deviation in fitted in-plane parameters and rib orientation parameters for all rib levels.

Rib	n	S_x mm	X_{Pk} mm per S_x	Y_{Pk} mm per S_x	ϕ_{pia} deg	B_p	B_d	α_{PH} deg	α_{LS} deg	α_{BH} deg
1	1444	71.0	0.384	0.521	81.7	−0.43	1.81	58.2	36.2	11.6
		±7.2	±0.061	±0.059	±9.3	±0.60	±1.16	±9.7	±7.0	±7.4
2	1665	110.9	0.318	0.621	111.8	−0.32	0.71	60.4	20.3	5.4
		±9.6	±0.048	±0.054	±8.6	±0.23	±0.55	±9.6	±4.6	±6.9
3	1681	141.7	0.344	0.588	116.8	−0.51	0.36	61.1	20.7	5.4
		±11.9	±0.041	±0.057	±8.3	±0.15	±0.42	±9.1	±3.9	±7.0
4	1661	166.8	0.322	0.527	115.4	−0.50	−0.05	60.3	22.9	6.9
		±13.7	±0.041	±0.053	±8.5	±0.16	±0.37	±8.8	±3.6	±7.3
5	1650	184.8	0.312	0.480	113.9	−0.51	−0.37	59.2	24.6	8.2
		±15.2	±0.041	±0.050	±8.7	±0.18	±0.35	±8.7	±3.4	±7.4
6	1659	197.3	0.297	0.439	112.0	−0.45	−0.51	57.6	28.0	10.7
		±16.2	±0.042	±0.049	±9.8	±0.22	±0.40	±8.6	±3.7	±7.3
7	1714	208.8	0.284	0.391	109.3	−0.35	−0.17	55.9	33.9	14.6
		±16.3	±0.043	±0.045	±11.3	±0.26	±0.66	±8.3	±4.3	±7.2
8	1780	209.1	0.297	0.364	104.8	−0.33	−0.22	53.7	39.9	16.6
		±16.0	±0.043	±0.039	±11.4	±0.29	±0.64	±8.0	±4.8	±7.5
9	1863	199.0	0.346	0.356	97.4	−0.51	−0.09	53.0	46.5	14.0
		±15.4	±0.041	±0.037	±11.4	±0.31	±0.59	±7.6	±5.3	±7.6
10	1905	183.7	0.372	0.329	90.0	−0.62	−0.09	51.4	56.1	11.2
		±15.1	±0.037	±0.035	±11.3	±0.35	±0.61	±7.0	±6.4	±7.9
11	1850	154.2	0.388	0.275	82.7	−0.69	0.59	49.4	69.9	10.4
		±17.4	±0.036	±0.036	±12.9	±0.56	±1.37	±5.9	±7.6	±9.0
12	1755	95.7	0.390	0.174	60.9	−1.29	1.37	53.3	94.0	14.6
		±29.1	±0.101	±0.045	±25.5	±1.66	±2.17	±8.5	±12.0	±17.9

Table A2 In-plane rib shape model with parameter coefficients predicted by demographics. Age (A) is in years, sex (S) is 0 for males and 1 for females, height (H) is in meters, weight (W) is in kilograms, along with the regression intercept (I).

	S_x					X_{Px}					Y_{Px}				
No.	I	$A_{E\text{-}3}$	$S_{E\text{-}1}$	$H_{E\text{-}1}$	$W_{E\text{-}3}$	$I_{E\text{-}3}$	$A_{E\text{-}5}$	$S_{E\text{-}3}$	$H_{E\text{-}3}$	$W_{E\text{-}5}$	$I_{E\text{-}2}$	$A_{E\text{-}5}$	$S_{E\text{-}3}$	$H_{E\text{-}3}$	$W_{E\text{-}5}$
1	**31**	**98**	**−24**	**190**	**40**	**415**	−23	4	−17	8	**62**	**−63**	−9	−36	−7
2	**56**	**129**	**−34**	**286**	13	**292**	16	−3	26	**−30**	**67**	**−83**	0	2	−7
3	**67**	**168**	**−39**	**403**	−9	**296**	**17**	7	**42**	**−42**	**63**	**−93**	−1	−2	13
4	**81**	**195**	**−61**	**469**	−18	**349**	−6	4	−0	**−31**	**57**	**−96**	1	−8	**24**
5	**88**	**237**	**−90**	**528**	−15	**398**	**−23**	2	**−39**	−11	**53**	**−104**	7	−17	**27**
6	**96**	**265**	**−102**	**562**	−37	**407**	**−48**	−1	**−54**	8	**49**	**−111**	6	−20	**37**
7	**106**	**283**	**−105**	**566**	−33	**437**	**−71**	−4	**−76**	**18**	**44**	**−109**	2	−16	**39**
8	**92**	**246**	**−106**	**651**	−14	**479**	**−74**	−2	**−94**	**20**	**45**	**−92**	−5	**−40**	**35**
9	**83**	**192**	**−104**	**648**	14	**481**	**−63**	1	**−70**	**18**	**41**	**−79**	−4	−24	**29**
10	**67**	**187**	**−93**	**628**	**55**	**467**	**−52**	**−8**	**−41**	7	**38**	**−70**	**−9**	−14	**11**
11	**38**	**168**	**−85**	**629**	**59**	**524**	**−48**	**−14**	**−62**	−0	**32**	**−57**	**−15**	−10	5
12	8	35	**−92**	**469**	**129**	**451**	**−48**	**−30**	−30	**33**	**10**	−7	−5	42	**15**

	ϕ_{pia}					B_p					B_d				
No.	I	$A_{E\text{-}3}$	$S_{E\text{-}1}$	$H_{E\text{-}1}$	$W_{E\text{-}3}$	$I_{E\text{-}2}$	$A_{E\text{-}4}$	$S_{E\text{-}2}$	$H_{E\text{-}2}$	$W_{E\text{-}4}$	$I_{E\text{-}2}$	$A_{E\text{-}4}$	$S_{E\text{-}2}$	$H_{E\text{-}2}$	$W_{E\text{-}4}$
1	**83**	**71**	10	−12	**−34**	−85	15	4	23	−8	165	**92**	−4	−28	22
2	**118**	**62**	**30**	−42	**−40**	**−48**	−5	**6**	9	−0	−5	**38**	−0	42	**−18**
3	**114**	**71**	**32**	−1	**−27**	**−28**	**−17**	0	−12	**9**	−22	10	6	37	**−15**
4	**110**	**78**	**41**	12	−23	**−32**	**−18**	−1	−12	**13**	50	−11	2	−22	**−14**

(continued)

Table 4. (continued)

	ϕ_{pia}					B_p					B_d				
No.	I	$A_{E\text{-}3}$	$S_{E\text{-}1}$	$H_{E\text{-}1}$	$W_{E\text{-}3}$	$I_{E\text{-}2}$	$A_{E\text{-}4}$	$S_{E\text{-}2}$	$H_{E\text{-}2}$	$W_{E\text{-}4}$	$I_{E\text{-}2}$	$A_{E\text{-}4}$	$S_{E\text{-}2}$	$H_{E\text{-}2}$	$W_{E\text{-}4}$
5	**100**	**83**	**48**	63	**−36**	**−34**	**−19**	−2	−6	4	23	**−22**	−1	−28	−3
6	**98**	**76**	**59**	73	**−65**	−23	**−13**	−2	−8	−2	12	**−27**	4	−27	−7
7	**95**	**81**	**66**	81	**−79**	**−43**	−3	−4	10	−7	−31	22	**19**	13	**−34**
8	**84**	**69**	**50**	**135**	**−94**	**−67**	−3	−5	26	−7	10	−4	**16**	1	**−47**
9	**80**	**42**	**47**	**123**	**−91**	**−55**	**−12**	−4	7	−1	65	**−29**	**13**	−19	**−40**
10	**69**	29	**32**	**154**	**−100**	−2	**−18**	**−9**	**−37**	**19**	32	2	−4	−19	−9
11	**66**	6	**40**	**126**	**−84**	−53	**−29**	**−22**	−14	**38**	**207**	**81**	**31**	**−134**	30
12	40	−52	−10	148	−5	−140	**65**	27	−7	−25	119	4	25	−22	50

	α_{PH}					α_{LS}					α_{BH}				
No.	$I_{E\text{-}1}$	$A_{E\text{-}3}$	$S_{E\text{-}2}$	$H_{E\text{-}1}$	$W_{E\text{-}3}$	I	$A_{E\text{-}3}$	$S_{E\text{-}2}$	$H_{E\text{-}1}$	$W_{E\text{-}3}$	$I_{E\text{-}1}$	$A_{E\text{-}3}$	$S_{E\text{-}1}$	$H_{E\text{-}1}$	$W_{E\text{-}3}$
1	**756**	**96**	**−358**	**−236**	**235**	**32**	**−76**	−26	**95**	**−92**	89	−18	−3	**77**	**−113**
2	**757**	**103**	**−350**	**−238**	**263**	**15**	**−33**	**−124**	**69**	**−52**	87	−7	−12	−1	**−25**
3	**770**	**94**	**−350**	**−243**	**271**	**19**	**−33**	**−80**	**47**	**−47**	62	−0	−2	13	**−35**
4	**752**	**88**	**−354**	**−235**	**272**	**24**	**−28**	**−121**	23	**−40**	93	12	1	6	**−48**
5	**740**	**86**	**−357**	**−235**	**274**	**30**	**−24**	**−161**	−3	**−27**	89	14	4	18	**−54**
6	**702**	**87**	**−318**	**−227**	**280**	**35**	−6	**−209**	−27	**−15**	107	**30**	4	25	**−70**
7	**706**	**88**	**−266**	**−236**	**271**	**41**	8	**−205**	−34	−6	90	**47**	1	**63**	**−88**
8	**664**	**85**	**−175**	**−222**	**261**	**46**	15	**−203**	−36	1	98	**54**	−9	**85**	**−119**
9	**670**	**91**	**−128**	**−224**	**243**	**57**	9	**−166**	**−65**	15	75	**28**	**−23**	**103**	**−136**
10	**601**	**102**	−78	**−182**	**210**	**70**	10	**−126**	**−101**	**45**	86	−18	**−31**	**95**	**−133**
11	**544**	**77**	−16	**−132**	**164**	**83**	25	−76	**−103**	**40**	65	**−34**	**−48**	**107**	**−123**
12	**631**	**49**	−113	**−117**	**96**	**116**	35	−81	**−113**	**−44**	146	−9	**−72**	101	**−160**

Subscript denotes scale factor. For example, $W_{E\text{-}3}$ indicates weight in kg scaled by 1×10^{-3}. Coefficients significantly different from zero at the $P < 0.01$ level are shown in bold.